Alveolar macrophage chromatin is uniquely modified to orchestrate host response to *Mycobacterium bovis* infection

Thomas Jonathan Hall [1], Douglas Vernimmen [2, *], John Andrew Browne [1], Michael P. Mullen [3], Stephen Vincent Gordon [4, 5], David Evan MacHugh [1, 4] and Alan Mark O'Doherty [1, 6, *]

[1] Animal Genomics Laboratory, UCD School of Agriculture and Food Science, College Dublin, Belfield, Dublin, D04 V1W8, Ireland.

[2] The Roslin Institute, University of Edinburgh, Easter Bush Campus, Midlothian, EH25 9RG, UK.

[3] Bioscience Research Institute, Athlone Institute of Technology, Dublin Road, Athlone, Co. Westmeath, N37 HD68, Ireland.

[4] UCD School of Veterinary Medicine, University College Dublin, Belfield, Dublin, D04 W6F6, Ireland.

[5] UCD Conway Institute of Biomolecular and Biomedical Research, University College Dublin, Belfield, Dublin, D04 V1W8, Ireland.

[6] Lead contact: Thomas Jonathan Hall, Thomas.Hall@ucdconnect.ie, ++353857168930

[*] Corresponding authors: alan.odoherty@ucd.ie and douglas.vernimmen@roslin.ed.ac.uk

Grant Support:

This study was supported by Science Foundation Ireland (SFI) Investigator Programme Awards (grant nos. SFI/08/IN.1/B2038 and SFI/15/IA/3154); a European Union Framework 7 Project Grant (no: KBBE-211602-MACROSYS); and an EU H2020 COST Action short

22 term scientific mission (STSM) grant (reference code: COST-STSM-ECOST-STSM-
23 CA15112-050317-081648).

24 Keywords: ChIP-seq, chromatin, macrophage, *Mycobacterium bovis*, tuberculosis

Highlights

- Comprehensive analysis of bovine alveolar macrophage (bAM) transcriptome and chromatin architecture revealed *Mycobacterium bovis* (*M. bovis*) induces genome-wide chromatin remodelling in bAM

- *M. bovis* induces transcriptional changes of immune response genes, associated with changes of histone modifications and RNA Polymerase II (PolII) occupancy

- GWAS integration of our ChIP study enabled the identification of important SNPs for bovine tuberculosis (bTB) susceptibility

45 **Graphical Abstract**

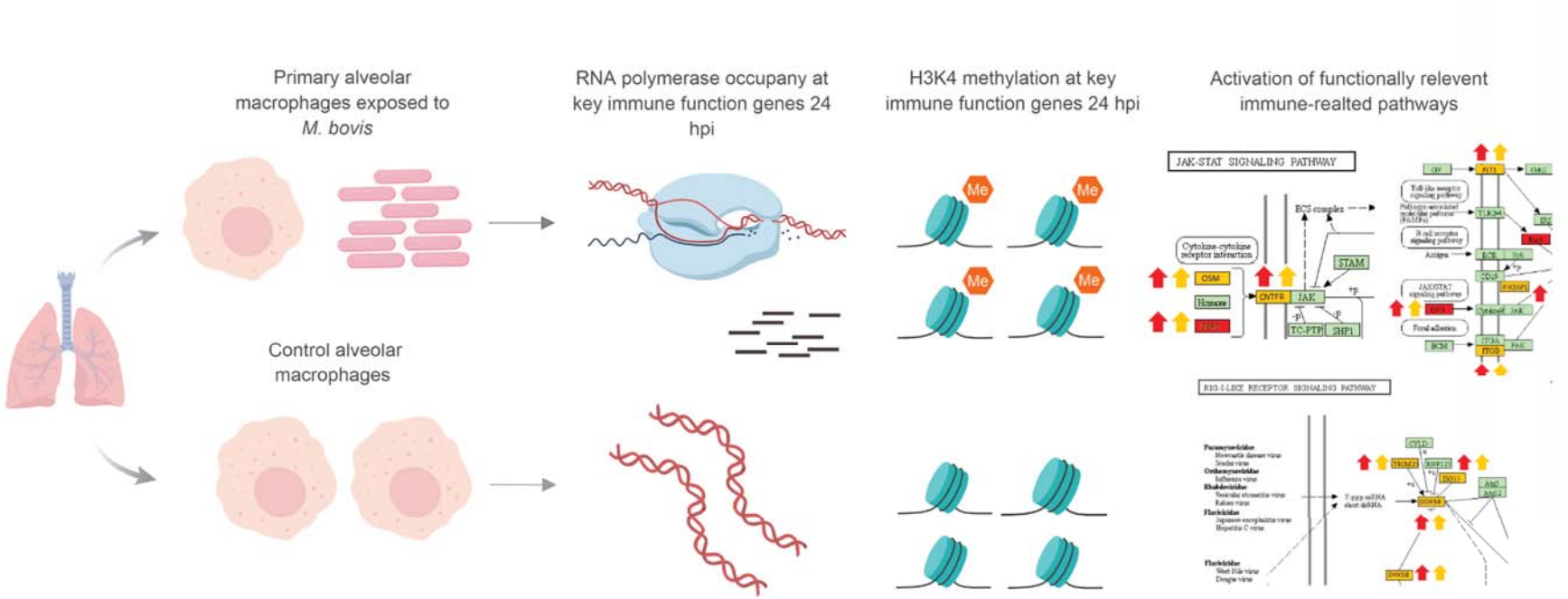

46

47

48

Summary

Mycobacterium bovis, the causative pathogen of bovine tuberculosis (bTB), induces extensive reprogramming of the macrophage transcriptome during infection. To identify key transcriptional changes in infected bovine alveolar macrophages (bAM), we have performed both gene expression (RNA-seq) and epigenomic (ChIP-seq) analyses using two key histone modification marks associated with activation (H3K4me3) and repression (H3K27me3). Together with RNA polymerase II (PolII) occupancy data, we show that reprogramming of the bAM transcriptome after *M. bovis* infection affects key immune response genes. Identification of these genes also facilitated integration of GWAS data, which identified genomic regions and SNPs significantly associated with resilience to infection with *M. bovis* in cattle.

Introduction

Bovine tuberculosis (bTB) is a chronic infectious disease of livestock, particularly domestic cattle (*Bos taurus* and *Bos indicus*), which causes more than $3 billion in losses to global agriculture annually (Steele, 1995; Waters et al., 2012). The disease can also significantly impact wildlife including, for example, several deer species, American bison (*Bison bison*), African buffalo (*Syncerus caffer*), the brushtail possum (*Trichosurus vulpecula*) and the European badger (*Meles meles*) (Fitzgerald and Kaneene, 2013; Gormley and Corner, 2017; Malone and Gordon, 2017; Palmer, 2013). The etiological agent of bTB is *Mycobacterium bovis*, a facultative pathogen with a genome sequence that is 99.95% to *M. tuberculosis*, the primary cause of human tuberculosis (TB) (Garnier et al., 2003). In certain agroecological milieus *M. bovis* can also cause zoonotic TB with serious implications for human health (Olea-Popelka et al., 2017; Thoen et al., 2016; Vayr et al., 2018).

Previous studies have shown that the pathogenesis of bTB disease is similar to TB disease in humans and many of the features of *M. tuberculosis* infection are also characteristic of *M. bovis* infection in cattle (Buddle et al., 2016; Waters et al., 2014; Williams and Orme, 2016). Transmission is via inhalation of contaminated aerosol droplets and the primary site of infection is the lungs where the bacilli are phagocytosed by alveolar macrophages, which normally can contain or destroy intracellular bacilli (Kaufmann and Dorhoi, 2016; Weiss and Schaible, 2015). Disease-causing mycobacteria, however, can persist and replicate within alveolar macrophages via a bewildering range of evolved mechanisms that subvert and interfere with host immune responses (Awuh and Flo, 2017; Cambier et al., 2014; de Chastellier, 2009; Schorey and Schlesinger, 2016). These mechanisms include: recruitment of cell surface receptors on the host macrophage; blocking of macrophage phagosome-lysosome fusion; detoxification of reactive oxygen and nitrogen intermediates (ROI and RNI); harnessing of intracellular nutrient supply and metabolism;

inhibition of apoptosis and autophagy; suppression of antigen presentation; modulation of macrophage signalling pathways; cytosolic escape from the phagosome; and induction of necrosis, which leads to severe immunopathology and shedding of the pathogen from the host (BoseDasgupta and Pieters, 2018; Chaurasiya, 2018; Ehrt and Schnappinger, 2009; Hussain Bhat and Mukhopadhyay, 2015; Queval et al., 2017; Stutz et al., 2018).

Considering the dramatic perturbation of the vertebrate macrophage by intracellular mycobacteria, we and others have demonstrated that bovine and human alveolar macrophage transcriptomes are extensively reprogrammed in response to infection with *M. bovis* and *M. tuberculosis* (Jensen et al., 2018; Lavalett et al., 2017; Malone et al., 2018; Nalpas et al., 2015; Papp et al., 2018; Vegh et al., 2015). These studies have also revealed that differentially expressed gene sets and dysregulated cellular networks and pathways are functionally associated with many of the macrophage processes described above that can control or eliminate intracellular microbes.

For many intracellular pathogens it is now also evident that the infection process involves alteration of epigenetic marks and chromatin remodelling that may profoundly alter host cell gene expression (Bierne et al., 2012; Hamon and Cossart, 2008; Niller and Minarovits, 2016; Rolando et al., 2015). For example, distinct DNA methylation changes are detectable in macrophages infected with the intracellular protozoan *Leishmania donovani*, which causes visceral leishmaniasis (Marr et al., 2014). Recent studies using cells with a macrophage phenotype generated from the THP-1 human monocyte cell line have provided evidence that infection with *M. tuberculosis* induces alterations to DNA methylation patterns at specific inflammatory genes (Zheng et al., 2016) and across the genome in a non-canonical fashion (Sharma et al., 2016).

With regards to host cell histones, the intracellular pathogen *Chlamydia trachomatis* secretes NEU, a SET domain-containing effector protein that functions as a histone

120 methyltransferase and induces chromatin modifications favourable to the pathogen (Pennini
121 et al., 2010). It has also been shown that *Legionella pneumophila*—the causative agent of
122 Legionnaires' disease—secretes a SET domain-containing histone methyltransferase, RomA,
123 which targets histone H3 to downregulate host genes and promote intracellular replication
124 (Rolando et al., 2013). In the context of mycobacterial infections, Yaseen et al. have shown
125 that the Rv1988 protein, secreted by virulent mycobacteria, localises to the chromatin upon
126 infection and mediates repression of host cell genes through methylation of histone H3 at a
127 non-canonical arginine residue (Yaseen et al., 2015). In addition, chromatin
128 immunoprecipitation sequencing (ChIP-seq) analysis of H3K4 monomethylation (a marker of
129 poised or active enhancers), showed that regulatory sequence motifs embedded in subtypes of
130 Alu SINE transposable elements are key components of the epigenetic machinery modulating
131 human macrophage gene expression during *M. tuberculosis* infection (Bouttier et al., 2016).

132 In light of the profound macrophage reprogramming induced by mycobacterial
133 infection, and previous work demonstrating a role for host cell chromatin modifications, we
134 have used ChIP-seq and RNA sequencing (RNA-seq) to examine gene expression changes
135 that reflect host-pathogen interaction in bovine alveolar macrophages (bAM) infected with *M.*
136 *bovis*. The results obtained support an important role for dynamic chromatin remodelling in
137 the macrophage response to mycobacterial infection, particularly with respect to M1/M2
138 polarisation. Genes identified from ChIP-seq and RNA-seq results were also integrated with
139 GWAS data to prioritise genomic regions and SNPs associated with BTB resilience. Finally,
140 the suitability of bAM for ChIP-seq assays and the results obtained demonstrate that these
141 cells represent an excellent model system for unravelling the epigenetic and transcriptional
142 circuitry perturbed during mycobacterial infection of vertebrate macrophages.

143

Results

M. bovis infection induces trimethylation of H3K4 at key immune function related loci in bovine alveolar macrophages

Previous studies have shown that bAM undergo extensive gene expression reprogramming following infection of *M. bovis* (Nalpas et al., 2015), with approximately one third of the genome significantly differentially expressed within bovine macrophages 24 hours after infection (Malone et al., 2018). Changes of this magnitude are comparable to those observed in previous experiments that have examined the chromatin remodelling that accompanies mycobacterial infection of macrophages, where trimethylation of lysine 4 of Histone H3 (H3K4me3) was shown to correlate with active transcription (Arts et al., 2018; Bouttier et al., 2016).

We used chromatin immunoprecipitation sequencing (ChIP-seq) to examine histone modification changes that occur after *M. bovis* infection of bAM from sex- and aged-matched Holstein-Friesian cattle. The aim was to determine genome-wide changes in the distribution of H3K4me3 and H3K27me3, and PolII occupancy at the response genes (Sims et al., 2003). After data quality control and filtering, ~760 million paired end reads were aligned to the UMD 3.1 bovine genome build at an average alignment rate of 96.23%. Correlation plots of genome-wide H3K4me3, H3K27me3 and PolII sequencing reads from infected and non-infected bAMs showed high correlation between samples (Pearson's correlation coefficient: 0.93–0.97) for all three ChIP-seq targets (supplementary figure 1); indicating that the observed differences in histone modifications between samples are limited and localised to specific regions of the genome.

Differential peaks between conditions were called, compared and visualised with IGV to determine where differences in H3K4me3, H3K27me3 and PolII occupancy occur between

control and infected bAM (Figure 1). ChIP seq peaks are defined as areas of the genome enriched by read counts after alignment to the reference genome.

Peak differences for H3K4me3 occurred at multiple locations across the genome and were estimated by the fold enrichment of a peak normalised against input control DNA that had not undergone antibody enrichment. Differential peaks in each condition were defined by several criteria: 1) the fold enrichment of each peak had to be larger than 10 in at least one condition (Landt et al., 2012); 2) the identified peaks had a *P*-value cut off of 0.05; 3) the peaks being compared in each condition were no more than 500 bp up- and downstream of each other; 4) the peaks were classified as different using log-likelihood ratios and affinity scores, with using MACS2 and diffBind, respectively; and 5) visual inspection of the tracks of the peaks confirmed the computationally determined differences in each condition.

Peaks that occurred in a particular sample indicate that H3K4me3 and PolII are highly correlated with condition (Figure 2A); this demonstrates that the differences in H3 modifications are a result of infection rather than genomic differences between animals. Analysis of genome-wide H3K4me3 revealed significant peak differences between control and infected samples at multiple sites in the genome under these criteria, with some of these differences occurring at the transcriptional start site of 233 genes. (Figure 2 A-D and supplementary figure 4). Supplementary figure 1 demonstrates that the differences in H3K4me3 and Pol II peaks are minor, with cells from both conditions sharing most peaks and differing by only 1.8–2.95% in peaks across the genome. Principal component analysis (PCA) of the H3K4me3 mark and PolII data indicated that these H3K4me3 and PolII peak differences are strongly associated with *M. bovis* infection of bAM (supplementary figure 3).

Changes in H3K4me3 are accompanied with immune related transcriptional reprogramming

Previous studies have shown that increased H3K4me3 is frequently accompanied by an increase in PolII occupancy and elevated expression of proximal genes (Barski et al., 2017; Clouaire et al., 2012). In the present study, we observed that H3K4me3 is accompanied by an increase in PolII occupancy (Figure 1 and supplementary figure 4). For a small number of genes (24 out of 233) where the H3K4me3 peak was larger in the control than the infected samples, PolII occupancy was greater in control bAM for 20 genes (83.3%) and greater in infected bAM for three genes (12.5%). Conversely, where the H3K4me3 peak was larger in the infected bAM, PolII occupancy was greater in the infected samples for 127 genes (60.4%) and greater in the control bAM for 14 genes (6.6%). The remaining 60 genes (25%) did not exhibit H3K4me-associated PolII occupancy in either control or infected samples. Figure 3A illustrates this trend, showing that PolII occupancy normally accompanies H3K4me3.

To establish if H3K4me3 mark patterns were correlated with changes in gene expression, control non-infected bAM and bAM infected *M. bovis* AF2122/97 from four animals 24 hpi (including the two animals used for ChIP-seq) were used to generate eight RNA-seq libraries. After quality control and filtering, ~250 million reads were mapped to the bovine genome, with 72% total read mapping, overall. RNA-seq analysis revealed 7,757 differentially expressed genes ($\log_2FC > 0$: 3723 genes; $\log_2FC < 0$: 4034 genes; FDR < 0.10). Of the 233 genes identified in the ChIP-seq analysis, 232 (99.6%) were differentially expressed with these criteria (see supplementary file 2). Of the genes that exhibited H3K4me3 peaks that were larger in the infected bAMs, 21 (10%) were downregulated and 189 (90%) were upregulated. Of the genes that exhibited larger H3K4me3 peaks in the control group, 22 (91.6%) were downregulated and 2 (8.4%) were upregulated (Figure 3A). This pattern of directional gene expression correlating with H3K4me3 for the control and infected samples is consistent with the literature (Barski et al., 2017; Clouaire et al., 2012).

Existing published RNA-seq data generated by our group using *M. bovis*-infected (n = 10) and control non-infected bAM (n = 10) at 24 hpi (Nalpas et al., 2015), was also examined in light of the results from the present study. For the 232 genes identified here, a Pearson correlation coefficient of 0.85 was observed for two data sets (Figure 3D), thus demonstrating that gene expression differences between *M. bovis*-infected and control non-infected bAM are consistent across experiments, even where samples sizes are markedly different.

Transcriptional reprogramming is coupled with differential microRNA expression

We have previously demonstrated that differential expression of immunoregulatory microRNAs (miRNAs) is evident in bAM infected with *M. bovis* compared to non-infected control bAM (Vegh et al., 2013; Vegh et al., 2015). To investigate the expression of miRNA in bAM used for the ChIP-seq analyses, miRNA was extracted and sequenced from the samples used for the RNA-seq analysis. After quality control and filtering, ~100 million reads were mapped to the bovine genome, with 79% total reads mapping, overall. Twenty-three differentially expressed miRNAs were detected at 24 hpi ($\log_2$FC > 0: 13; $\log_2$FC < 0: 10; FDR < 0.10). Of the 232 genes identified in the ChIP-seq/RNA-seq analysis, 93 are potential targets for the 23 differentially expressed miRNAs (supplementary data 3). Further examination revealed that multiple immune genes, such as *BCL2A1* (bta-mir-874), *ARG2(*bta-mir-101), *STING* (bta-mir-296-3p) and *STAT1(*bta-mir-2346), are potential regulatory targets for these miRNAs (Figure 3B). This observation therefore supports the hypothesis that miRNAs function in parallel with chromatin modifications to modulate gene expression in response to infection by *M. bovis*.

The H3K4me3, PolII, K27me3 and RNA-seq data were subsequently integrated to evaluate the relationship between histone modifications and gene expression changes. Three

dimensional plots were generated to visualize the global differences between H3K4me3, PolII and gene expression in infected and non-infected bAM (Figure 3D). These plots show that reduction of H3K4me3 in infected cells is associated with a decrease in gene expression and an absence of PolII occupancy. Genome-wide H3K27me3 was also investigated to determine whether methylation of this residue was altered in response to *M. bovis* infection and if it was related to gene expression. No significant differences for H3K27me3 between control and infected bAM were detected, indicating that repression of gene expression through H3K27me3 does not play a role in the bAM response to *M. bovis at 24hpi*. However, supplementary figure 2 indicates that presence of a H3K37me3 peak in both control and infected cells at the TSS of a H3k4me3 enriched gene correlated well with a lower or complete lack of Pol II occupancy.

Pathway analysis reveals H3K4me3 marks are enriched for key immunological genes

To identify biological pathways associated with genes identified through the ChIP-seq analyses, we integrated the ChIP-seq, RNA-seq and miRNA-seq data and created a list of 232 genes that were present in each data set. Pathway analyses were carried out using three pathway tools: Ingenuity Pathway Analysis (IPA), Panther and DAVID (Huang da et al., 2009; Kramer et al., 2014; Thomas et al., 2003). IPA revealed an association with *respiratory illness* and the *innate immune response* (supplementary file 2). Panther was used to examine the gene ontology categories of the 232 genes (Figure 4A); this revealed enrichment for metabolic processes, response to stimuli and cellular processes, indicating that increased H3K4me3 in response to *M. bovis* infection occurs at TSS of genes associated with the immune response.

The final part of the pathway analysis was performed using DAVID (Huang da et al., 2009). DAVID uses a list of background genes and query genes (in this case the 232 common

genes across data sets) and identifies enriched groups of genes with shared biological functions. The DAVID analysis demonstrated that the 232 genes are involved in several signalling pathways, including the PI3K/AKT/mTOR, JAK-STAT and RIG-I-like signalling pathways (Figure 4B and the top 10 pathways are detailed in supplementary file 3).

GWAS integration prioritises bovine SNPs associated with resilience to *M. bovis* infection

Previous work used high-density SNP (597,144 SNPs) data from 841 Holstein-Friesian bulls for a genome-wide association study (GWAS) to detect SNPs associated with susceptibility/resistance to *M. bovis* infection (Richardson et al., 2016). Using a permutation-based approach to generate null SNP distributions, we leveraged these data to show that genomic regions within 100 kb up- and downstream of each of the 232 genes exhibiting differential H3K4me3 ChIP-seq peaks are significantly enriched for additional SNPs associated with resilience to *M. bovis* infection.

In total, 12,056 SNPs within the GWAS data set were located within 100 kb of the 232 H3K4me3 genes. Of these SNPs, up to 26 were found to be significantly associated with bTB susceptibility, depending on the distance interval of each gene. Interestingly, 22 SNPs found within 25 kb of 11 genes were found to be most significant at P and q values < 0.05, with declining significance of association as the region extended beyond 25 kb (Figure 4C and supplementary file 3). Significant SNPs were detected in proximity to the following genes: *SAMSN1, CTSL, TNFAIP3, CLMP, ABTB2, RNFT1, MIC1, MIC2, EDN1, ARID5B,* all of which had significant differential enrichment of H3K4me3.

Discussion

H3K4me3 marks occur at key immune genes

Our study has generated new information regarding host-pathogen interaction during the initial stages of *M. bovis* infection. We demonstrate that chromatin is remodelled through differential H3K4me3 and that PolII occupancy is altered at key immune genes in *M. bovis*-infected bAM. This chromatin remodelling correlates with changes in the expression of genes that are pivotal for the innate immune response to mycobacteria (Alcaraz-Lopez et al., 2017; Malone et al., 2018; Nalpas et al., 2015). Our work supports the hypothesis that chromatin modifications of the host macrophage genome play an essential role during intracellular infections by mycobacterial pathogens (Cheng et al., 2014; LaMere et al., 2016).

The top pathways identified were the JAK-STAT signalling pathway, PI3K/AKT/mTOR signalling pathway and the RIG-I-like receptor signalling pathway. In mammals, the JAK-STAT pathway is the principal signalling pathway that modulates expression of a wide array of cytokines and growth factors, involved in cell proliferation and apoptosis (Rawlings et al., 2004). The JAK-STAT signalling pathway and its regulators are also associated with coordinating an effective host response to mycobacterial infection (Cliff et al., 2015; Manca et al., 2005). Two JAK-STAT associated stimulating factors and a ligand receptor that exhibited increased H3K4me3 marks in infected samples were encoded by the *OSM*, *CSF3* and *CNTFR* genes, respectively (Marino and Roguin, 2008; Pastuschek et al., 2015). *OSM* has previously been shown to be upregulated in cells infected with either *M. bovis* or *M. tuberculosis* (Nalpas et al., 2015; O'Kane et al., 2008; Polena et al., 2016). Our work shows that this increased expression in response to mycobacteria is facilitated by H3K4me3-mediated chromatin accessibility. The protein encoded by *CSF3* has also been implicated as an immunostimulator in the response to mycobacterial infection due to its role in granulocyte and myeloid haematopoiesis (Martins et al., 2010). *CNTFR* encodes a ligand receptor that stimulates the JAK-STAT pathway and shows increased expression in other studies of mycobacterial infection (Malone et al., 2018; Nalpas et al., 2015). Following

312 stimulation of *JAK* through ligand receptor binding, *STAT1* expression is increased. STAT1,
313 a signal transducer and transcription activator that mediates cellular responses to interferons
314 (IFNs), cytokines and growth factors, is a pivotal JAK-STAT component and a core
315 component in the response to mycobacterial infection (Tsumura et al., 2012). Here, the TSS
316 of *STAT1* was associated with an increased deposition of H3K4me3. Interestingly,
317 upregulation of *STAT1* was associated with a downregulation of bta-miR-2346, predicted to
318 be a negative regulator of STAT1 (see supplementary file 3). Overall, these results show that
319 major components of the JAK-STAT pathway undergo chromatin remodelling mediated via
320 H3K4me3, thereby facilitating activation and propagation of the JAK-STAT pathway
321 through chromatin accessibility.

322 Key genes encoding components of the PI3K/AKT/mTOR pathway, such as *IRF7*,
323 *RAC1* and *PIK3AP1*, were also identified as having increased H3K4me3 in *M. bovis* infected
324 macrophages. PI3K/AKT/mTOR signalling contributes to a variety of processes that are
325 critical in mediating aspects cell growth and survival (Yu and Cui, 2016).
326 Phosphatidylinositol-3 kinases (PI3Ks) and the mammalian target of rapamycin (mTOR) are
327 integral to coordinating innate immune defences (Weichhart and Saemann, 2008). The
328 PI3K/AKT/mTOR pathway is an important regulator of type I interferon production via
329 activation of the interferon-regulatory factor 7, IRF7. RAC1 is a key activator of the
330 PI3K/AKT/mTOR pathway and, in its active state, binds to a range of effector proteins to
331 regulate cellular responses such as secretory processes, phagocytosis of apoptotic cells, and
332 epithelial cell polarization (Yip et al., 2007). In addition, *in silico* analysis of our
333 differentially expressed miRNAs predicted that several miRNAs, such as bta-miR-1343-3p,
334 bta-miR-2411-3p and bta-miR-1296, regulate *RAC1*. *PIK3AP1* expression was also
335 increased, in line with previous mycobacterial infection studies (Malone et al., 2018; Nalpas
336 et al., 2015). Hence as observed with the JAK-STAT pathway, H3K4me3 at these key

337 PI3K/AKT/mTOR pathway genes acts to regulate the innate response to mycobacterial
338 infection.

339 Initiation of the RIG-I-like receptor signalling pathway generally occurs following viral
340 infection through sensing of viral RNAs by cytoplasmic RIG-I-like receptors (RLRs) and
341 activation of transcription factors that drive production of type I IFNs (Loo and Gale, 2011).
342 A number of bacterial species induce type I IFN independently of TLRs, potentially through
343 the RIG-I-like pathway (Charrel-Dennis et al., 2008; Dixit and Kagan, 2013). While type I
344 IFNs have a well characterised role in the inhibition of viral replication, their role during
345 bacterial infection is less well defined (Boxx and Cheng, 2016; Mancuso et al., 2007;
346 O'Connell et al., 2004). In humans and mice, *M. tuberculosis*-induced type I IFN is associated
347 with TB disease progression and impairment of host resistance (Berry et al., 2010; Manca et
348 al., 2001; Mayer-Barber et al., 2014). In our study, genes encoding multiple components of
349 the RIG-I-like receptor signalling pathway, such as *TRIM25, ISG15, IRF7* and *IKBKE,* were
350 enriched for K4me3 and PolII occupancy in *M. bovis*-infected bAM. These results
351 demonstrate that the RIG-I-like pathway activation in *M. bovis*-infected bAM is driven, to a
352 large extent, by reconfiguration of the host chromatin.

353 H3K4me3 enriched loci are also flanked by genomic polymorphisms associated with
354 resilience to *M. bovis* infection. Integration of our data with GWAS data from 841 bulls that
355 have robust phenotypes for bTB susceptibility/resistance revealed 22 statistically significant
356 SNPs within 25 kb of 11 H3K4me3 enriched genes. Most of these genes are involved in host
357 immunity, with *CTSL, TNFAIP3,* and *RNFT1* directly implicated in the human response to *M.*
358 *tuberculosis* infection (Meenu et al., 2016; Nepal et al., 2006; Silver et al., 2009). The
359 reprioritisation of genomic regions and array based SNPs using integrative genomics
360 approaches will be relevant for genomic prediction and genome-enabled breeding and may

facilitate fine mapping efforts and the identification of targets for genome editing of cattle resilient to bTB.

H3K4me3 deposition at host macrophage genes may indicate immunological evasion by *M. bovis*

The present study has revealed elevated H3K4me3 deposition and PolII occupancy at key immune genes that are involved in the innate response to mycobacterial infection. In addition, we also identified a number of immune genes that had differential H3K4me3 and expression, where the expression change may be detrimental to the host macrophage response to infection. An example of this is *ARG2*, which exhibited increased H3K4me3 deposition, PolII occupancy and expression (LogFC : 3.415, Q-value : 7.52099E-16) in infected cells. However, it is also interesting to note that the integrated expression output of *ARG2* may also be determined by the bta-miR-101 miRNA, a potential silencer of *ARG2* expression, which was observed to be upregulated in infected cells. Elevated levels of Arginase 2, the protein product of the *ARG2* gene has previously been shown to shift macrophages to an M2 phenotype (Hardbower et al., 2016; Lewis et al., 2011), which are anti-inflammatory and exhibit decreased responsiveness to IFN-gamma and decreased bactericidal activity (Huang et al., 2015). Hence, it may be hypothesised that *M. bovis* infection triggers H3K4me3 deposition at the TSS of *ARG2* to drive an M2 phenotype and generate a more favourable niche for the establishment of infection. Similar to *ARG2*, increased expression of *BCL2A1* in *M. bovis*-infected bAM may also facilitate development of a replicative milieu for intracellular mycobacteria. Increased expression of *BCL2A1* is associated with decreased macrophage apoptosis (Vogler, 2012), which would otherwise restrict replication of intracellular pathogens.

384 The *STING* (*TMEM173*) non-infected bAM and decreased concomitant expression in
385 *M.* bovis-infected bAM. *TMEM173* encodes transmembrane protein 173, which drives IFN
386 production and as such is a major regulator of the innate immune response to viral and
387 bacterial infections, including *M. bovis* and *M. tuberculosis* (Malone et al., 2018; Manzanillo
388 et al., 2012; McNab et al., 2015). Downregulation of *TMEM173* may signpost that *M. bovis* is
389 actively reducing or blocking methylation of H3K4 at this gene in infected macrophages,
390 thereby enhancing its intracellular survival. in this regard, we have recently shown that
391 infection of bAM with *M. tuberculosis*, which is attenuated in cattle, causes increased
392 *TMEM173* expression compared to infection with *M. bovis* (Malone et al., 2018).

393 The molecular mechanisms that pathogens employ to manipulate the host genome to
394 subvert or evade the immune response are yet to be fully elucidated. Hijacking the hosts own
395 mechanisms for chromatin modulation is one potential explanation that has garnered focus in
396 recent years (Hamon and Cossart, 2008; Rolando et al., 2015). These modulations of the host
397 chromatin in bAMs may be mediated through *M. bovis*-derived signals transmitted through
398 bacterial metabolites, RNA-signalling or secreted peptides (Sharma et al., 2015; Silmon de
399 Monerri and Kim, 2014; Woo and Alenghat, 2017; Yaseen et al., 2015).

400 **Conclusion**

401 Using transcriptomics and epigenomics, we have identified the host response genes
402 following infection with *M. bovis*. We have shown that reprogramming of the alveolar
403 macrophage transcriptome occurs mainly through increased deposition of H3K4me3at key
404 immune function genes, with additional gene expression modulation via miRNA differential
405 expression. We have also indicated that alveolar macrophages infected with M. bovis exhibit
406 differentially expressed genes (in regions with modified chromatin) that are enriched for
407 significant SNPs from GWAS data for BTB resilience. Our data support the hypothesis that

the pathogens hijack host chromatin, through manipulation of H3K4me3, to aid their subversion of the host immune response.

Materials and Methods

Ethics Statement

All animal procedures were performed according to the provisions of the Cruelty to Animals Act of 1876 and EU Directive 2010/63/EU. Ethical approval was obtained from the University College Dublin Animal Ethics Committee (protocol number AREC-13-14-Gordon).

Preparation and infection of bAMs

Alveolar macrophages and *M. bovis* 2122 were prepared as described previously (Magee et al., 2014) with minor adjustments, 2×10^6 macrophages were seeded in 60 mm tissue culture plates and challenged with *M. bovis* at an MOI of 10:1 (2×10^7 bacteria per plate) for 24 h; parallel non-infected controls were prepared simultaneously.

Preparation of nucleic acids for sequencing

Sheared fixed chromatin was prepared exactly as described in the truChIP™ Chromatin Shearing Kit (Covaris) using 2×10^6 macrophage cells per AFA tube. Briefly, cells were washed in cold PBS and 2.0 ml of fixing Buffer A was added to each plate, to which 200 µl of freshly prepared 11.1% formaldehyde solution was added. After 10 min on a gentle rocker the crosslinking was halted by the addition of 120 µl of quenching solution E, cells were washed with cold PBS, released from the plate using a cell scraper and re-suspended in 300 µl Lysis Buffer B for 10 min with gentle agitation at 4^{o}C to release the nuclei. The nuclei were pelleted and washed once in Wash Buffer C and three times in Shearing Buffer D3 (X3) prior to been resuspended in a final volume of 130 µl of Shearing Buffer D3. The nuclei were transferred to a micro AFA tube and sonicated for 8 min each using the Covaris E220e as per the manufacturer's instructions. Chromatin immunoprecipitation of sonicated DNA samples

was carried out using the Chromatin Immunoprecipitation (ChIP) Assay Kit (Merck KGaD) and anti-H3K4me3 (05-745R) (Merck KGaD), Pol II (H-224) (Santa Cruz Biotechnology, Inc.) or anti-H3K27me3 (07-449) (Merck KGaD) as previously described (Vernimmen et al., 2011). RNA was extracted from infected (n = 4) and control (n = 4) bAM samples using the RNeasy Plus Mini Kit (Qiagen) as previously described (O'Doherty et al., 2012). All 8 samples exhibited excellent RNA quality metrics (RIN >9).

Sequencing

Illumina TruSeq Stranded mRNA and TruSeq Small RNA kits were used for mRNA-seq and small RNA-seq library preparations and the NEB Next Ultra ChIPseq Library Prep kit (New England Biolabs) was used for ChIP-seq library preparations. Pooled libraries were sequenced by Edinburgh Genomics (http://genomics.ed.ac.uk) as follows: paired-end reads (2 × 75 bp) were obtained for mRNA and ChIP DNA libraries using the HiSeq 4000 sequencing platform and single-end read (50 bp) were obtained for small RNA libraries using the HiSeq 2500 high output version 4 platform.

ChIP-seq bioinformatics

Computational analyses for all bioinformatic processes were performed on a 72-CPU compute server with Linux Ubuntu (version 16.04.4 LTS). An average of 54 M paired end 75bp reads were obtained for each histone mark. At each step of data processing, read quality was assessed via FastQC (version 0.11.5) (Andrews, 2016). Any samples that indicated adapter contamination were trimmed via Cutadapt (version 1.15) (Martin, 2011). Raw read correlation plots were generated via EaSeq (version 1.05) (Lerdrup et al., 2016). The raw reads were aligned to UMD 3.1.1 bovine genome assembly using Bowtie2 (version 2.3.0) (Langmead and Salzberg, 2012). The mean alignment rate for the histone marks was 96.23%. The resulting SAM files were converted and indexed into BAM files via Samtools (version

458 1.3.1) (Li et al., 2009). After alignment, samples were combined and sorted into 14 files,
459 based on the animal (A1 or A2), the histone mark (K4/K27/PolII) and treatment (control or
460 infected) i.e. A1-CTRL-K4. Peaks were called by using alignment files to determine where
461 the reads have aligned to specific regions of the genome, and then comparing that alignment
462 to the input samples as a normalization step.

463 The peak calling was carried out via MACS (version 2.1.1.20160309) (Feng et al.,
464 2011). The K4me3 mark was called in sharp peak mode and K27me3 and Pol II were called
465 in broad peak mode, as per the user guide. Peak tracks were generated in macs and visualized
466 with the Integrative Genome Viewer (version 2.3) (Thorvaldsdottir et al., 2013). Union peaks
467 were generated by combining and merging overlapping peaks in all samples for each histone
468 mark. Differential peak calling was called via macs using the bdgdiff function. Peaks images
469 were generated by visually assessing all three marks in tandem across the entire bovine
470 genome with IGV. The significance of peaks was determined by sorting peaks for each mark
471 in each treatment by *P* value and then fold enrichment with a cut-off of 2 and a *P* value
472 threshold of 0.05 (Wilbanks and Facciotti, 2010). Peaks from each animal in each condition
473 for each mark were cross referenced with the IGV images and differential peak caller to
474 determine a difference in fold enrichment for each observed peak difference between
475 conditions. This required comparing peak start and end sites, chromosomes, *P* and *q* values
476 for each summit, summit locations and normalised fold enrichment of a peak against the
477 input sample (see supplementary file 1 for peak sets). Any peaks that exhibited a difference
478 of 4 or greater fold enrichment, a *P* value of less than 0.05, an FDR (*q* value) less than 0.05
479 and that were also identified by the differential peak caller were selected for further analysis
480 (see supplementary file 1 for peaks at TSS that met some but not all of the above criteria).
481 Peaks that were then classified to be different between conditions in all three data sets were
482 examined to determine their proximity to TSS. Differential peaks were also called using the

R package DiffBind (version 2.80) (Stark and Brown, 2011). DiffBind includes functions to support the processing of peak sets, including overlapping and merging peak sets, counting sequencing reads overlapping intervals in peak sets, and identifying statistically significantly differentially bound sites based on evidence of binding affinity (measured by differences in read densities, see supplementary info 1). For H3K27me3 DiffBind differential peak calling, the initial MACS2 peak list, consisting of 64,264 total peaks (see supplementary info 1), was merged and reduced to a smaller group of larger, broader peaks to reduce noise and false positive discovery (Figure 2B).

RNA-seq bioinformatics analysis

An average of 44 M paired end 75 bp reads were obtained for each of the eight samples (four control, four infected). Adapter sequence contamination and paired-end reads of poor quality were removed from the raw data. At each step, read quality was assessed with FastQC (version 0.11.5). Any samples that indicated adapter contamination were trimmed via Cutadapt (version 1.15). The raw reads were aligned to the UMD 3.1.1 bovine transcriptome using Salmon (version 0.8.1) (Patro et al., 2017). Aligned reads were also counted in Salmon and the resulting quantification files were annotated at gene level via tximport (version 3.7) (Soneson et al., 2015). The annotated gene counts were then normalised and differential expression analysis performed with DESeq2 (version 1.20.0) (Love et al., 2014), correcting for multiple testing using the Benjamini-Hochberg method (Benjamini and Hochberg, 1995). Genes identified from ChIP-seq as exhibiting differential histone modifications were cross referenced with the RNA-seq data set to determine significant $\log_2$FC between *M. bovis*-infected and control non-infected. Additionally, this RNA-seq data was cross referenced with RNA-seq data from a previous study that investigated bAM infected with *M. bovis* (Nalpas et al., 2015).

miRNA-seq bioinformatics analysis

A mean of 26 M paired-end 50 bp reads were obtained for each of the eight samples (four control, four infected). At each step of data processing, read quality was assessed via fastqc (version 0.11.5). Any samples that exhibited adapter contamination were trimmed via Cutadapt (version 1.15) and all reads smaller than 17 bp were removed from the analysis. Raw reads were mapped to UMD3.1 using Bowtie (version 1.2.2). miRNA detection, identification and quantification was carried out with mirdeep2 (version 0.0.91). Isoform analysis was also performed using mirdeep2. Differential expression analysis was performed using DESeq2, correcting for multiple testing with the Benjamini-Hochberg method. Any miRNAs that were significantly differentially expressed (FDR < 0.10) were selected for further analysis. To determine if significantly differentially expressed miRNAs target genes selected in the ChIP seq analysis, miRmap (Vejnar and Zdobnov, 2012) was used to predict the likelihood a specific miRNA targets one or more of the genes based on three criteria: delta G binding, probability exact and phylogenetic conservation of seed site, which is then combined into a single scoring metric (miRmap score). Any predicted gene targets with miRmap score ≥ 0.70 were included in the analysis (see supplementary info 3). All three datasets have been submitted to Gene Expression Omnibus (GEO) with accession number GSE116734.

Pathway analysis

Pathway analysis was carried out on any gene that had a differential peak between control and infected samples. Pathway analysis and gene ontology was carried out by DAVID (version 6.8), Ingenuity pathway analysis (01-13) and PANTHER (version 13.1) (Kramer et al., 2014; Mi et al., 2017). KEGG pathways were selected by choosing pathways that had the highest amount of genes identified in the ChIP seq data and had a FDR < 0.05.

Integration of GWAS data.

BTB GWAS results previously generated by Richardson et al 2016 were analysed to determine if subsets of SNPs selected according to their distance to H3K4me3 and PolII active loci were enriched for significant associations to bTB susceptibility. The nominal P values used in this study were generated using single snp regression analysis in a mixed animal model as described previously (Richardson et al 2016). In summary, high-density genotypes (n = 597,144) of dairy bulls (n = 841) used for artificial insemination were associated with deregressed estimated breeding values for bTB susceptibility that had been calculated from epidemiological information on 105,914 daughters and provided by the Irish Cattle Breeding Federation (ICBF). In this study, the significance of the distribution of SNP nominal p values (from Richardson et al 2016) within and up to 100kb up and downstream to genes identified as having differential H3K4me3 and PolII activity on bTB susceptibility were estimated in R using q value (FDRTOOL) and permutation analysis (custom scripts). Either 1000 or 10000 samplings (with replacement) from the HD GWAS p value dataset (n = 597,144) representing the size of each of selected SNP subsets were generated. Q values for each SNP p value subset and all its permuted equivalents (1000 or 10000) were calculated using the FDRTOOL library in R. The subsequent significance level (Pperm) assigned to each of the SNP subsets was equivalent to the proportion of permutations in which at least the same number of q values <0.05 as the SNP subset were obtained, i.e. by chance. 10000 permutations were carried out in the case when none of the 1000 permutations resulted in an occurrence of at least the number of q values < 0.05 as contained in its SNP subset.

552 **Figure legends**

553 **Figure 1. Track visualization of M. bovis induced H3K4me3 and PolII occupancy with**
554 **relative change in expression at three immune response associated genes.**

555 Examples of signal tracks illustrating peaks of H3K27me3 (top two tracks), H3K4me3
556 (middle two tracks) and PolII (bottom two tracks) in infected (red) and non-infected (blue)
557 bovine alveolar macrophages, with the bovine reference genome on the bottom of each panel
558 reading left to right. Accompanying each track image is the expression of the corresponding
559 gene, with normalised counts of infected cells in red and control in blue. The *ARG2* gene
560 exhibited an increase in H3K4me3 at 24 hpi as evidenced by the larger red H3K4me3 and red
561 PolII peaks. The *IFITM2* gene also exhibited larger H3K4me3 and PolII peaks in infected
562 samples; however, in contrast to this, *SIRT3*, which is located ~20kb upstream from *IFITM2*
563 gene, had no significant change in either peak. *STING* (*TMEM173*) exhibits an opposite
564 pattern to most genes identified as having differential H3K4me3, where a larger peak is
565 observed in control samples rather than infected.

566 **Figure 2. *M.bovis* induced histone modifications occur genome wide at key immune loci.**

567 (**A**) Correlation heatmaps of differential peaks for H3K4me3, H3K27me3 and PolII. Every
568 peak location that is not consistent between each animal in each condition (i.e. a peak only
569 occurs in the control group) is compared to determine if these inconsistent peaks are
570 correlated with the animal or the condition. The differential peaks in H3K4me3 and PolII
571 correlate highly with condition, whereas there was no significant global differences in the
572 distribution of H3K27me3. (**B**) Venn diagrams of differential peaks for H3K4me3,
573 H3K27me3 and PolII. Each condition shares the majority of peaks. Where differences occur
574 at TSS of genes, these genes are frequently associated with immune function. (**C**) Volcano
575 plots of differential peaks for H3K4me3 and PolII. The y-axis shows significance as FDR and

576 the x-axis indicates increase in affinity for control (left) and infected (right). Significant sites
577 are denoted in blue. (**E**) Boxplots of differential peaks for H3K4me3 and PolII. Infected bAM
578 are shown in red and control bAM are shown in blue. The left two boxes of each plot show
579 distribution of reads over all differentially bound sites in the infected and control groups. The
580 middle two boxes of each plot show the distribution of reads in differentially bound sites that
581 increase in affinity in the control group. The far right boxes in each plot show the distribution
582 of reads in differentially bound sites that increase in affinity in the infected group.

583 **Figure 3. H3K4me3 is accompanied by functional changes in PolII occupancy, gene**
584 **expression and gene regulation.**

585 (**A**) Scatter plots of H3K4me3 against PolII occupancy and gene expression. The first plot is
586 the difference of peaks for H3K4me3 between conditions, ranging from negative to positive
587 values, with negative being a larger peak in the control samples (blue dots) and the positive
588 values being a larger peak in the infected samples (red dots), on the y-axis. The x-axis
589 represents the log_2 fold change for each of the 232 genes, with each gene as a single data
590 point. The second plot also has H3K4me3 on the y-axis but with peak differences in PolII on
591 the x-axis, with negative and positive values corresponding to greater occupancy in the
592 control and infected samples, respectively. The final plot shows log_2 fold change relative to
593 PolII occupancy. (**B**) Plots of normalised miRNA-seq counts. Each plot represents the
594 normalised counts of a miRNA that was detected as exhibiting differential expression. Bta-
595 miR-101 interacts with *ARG2*, bta-miR-296-3p with *STING* (*TMEM173*), bta-miR-874 with
596 *BCL2A1* and bta-miR-2346 with *STAT1*. Red bars indicate infected and blue represent control
597 samples. (**C**) Correlation and Venn diagram for both RNA-seq studies. The x-axis of the
598 scatter plot represents the log_2 fold change for each of the 232 genes from this study and the
599 y-axis represents the log_2 fold change for each of the 232 genes from the previous study
600 (Nalpas et al., 2015). The Venn diagram shows the global overlap of differentially expressed

genes from both studies with an FDR cut off of <0.1. (**D**) 3-D plots for all three data sets. A combination of all three scatter plots from Figure 2A. Data points are genes. Blue genes are those that exhibited greater H3K4me3 in control bAM, red exhibited greater H3K4me3 in infected bAM.

Figure 4. Gene ontology enrichment and pathway analysis.

(**A**) Gene ontology pie charts generated through PANTHER pathway analysis. 232 genes cluster by gene ontology under three main categories: *Biological process*, *Cellular component* and *Molecular function*. (**B**) KEGG pathway images containing genes identified from the ChIP-seq and RNA-seq analysis. Gene symbols coloured in yellow were identified in the ChIP-seq and RNA-seq analysis. Gene symbols coloured in red were also targeted by one or more differentially expressed miRNAs. Up or down red arrows indicate greater H3K4me3 in infected or control, respectively. Up or down yellow arrows indicate log_2 fold change increase or decrease of the associated gene, respectively. (**C**) Line graph showing different genomic ranges from genes that are enriched for significant SNPs from GWAS data for BTB resilience. The bars represent the number of SNPs that occupy each range from each ChIP-seq enriched gene, with more SNPs correlating with a greater distance. The blue plotted line represents the negative $\log_{10}$ probability that the significant SNPs found at each distance at 0.05 FDR *q* value are significant by chance, with SNPs at 25 kb exhibiting the lowest probability. The null SNP *P* value distribution for each data point was generated from 1000 permutations of random SNPs corresponding to the number of SNPs observed in a particular genomic range.

Acknowledgments

This study was supported by Science Foundation Ireland (SFI) Investigator Programme Awards (grant nos. SFI/08/IN.1/B2038 and SFI/15/IA/3154) and a European Union Framework 7 Project Grant (no: KBBE-211602-MACROSYS). The authors would also like to thank FAANG–Europe for awarding A.M.O.D. a short term scientific mission (STSM) grant (reference code: COST-STSM-ECOST-STSM-CA15112-050317-081648). We would like to acknowledge Edinburgh Genomics for generation of sequencing data.

Author Contributions

Conceptualization, A.M.O.D., D.E.M. and T.J.H.; Software & Formal Analysis, T.J.H. and M.P.M.; Investigation, A.M.O.D., D.V. and J.A.B.; Resources, D.E.M., S.V.G. and D.V.; Data Curation, T.J.H.; Writing – original draft, T.J.H, A.M.O.D. and D.E.M.; Writing – review and editing, D.V., S.V.G and M.P.M.; Supervision and Project Administration, D.E.M. and A.M.O.D.; Funding Acquisition; D.E.M, S.V.G, D.V. and A.M.O.D.

Declaration of Interests

The authors declare no competing interests.

644 **References**

645 Alcaraz-Lopez, O.A., Garcia-Gil, C., Morales-Martinez, C., Lopez-Rincon, G., Estrada-
646 Chavez, C., Gutierrez-Pabello, J.A., and Esquivel-Solis, H. (2017). Divergent macrophage
647 responses to *Mycobacterium bovis* among naturally exposed uninfected and infected cattle.
648 Immunol. Cell Biol. 95(5), 436-442. Published online 2016/11/12 DOI:
649 10.1038/icb.2016.114.
650 Andrews, S., 2016. FastQC: a quality control tool for high throughput sequence data.
651 Bioinformatics Group, Babraham Institute, Babraham Research Campus, Cambridge, UK.
652 Arts, R.J.W., Moorlag, S., Novakovic, B., Li, Y., Wang, S.Y., Oosting, M., Kumar, V.,
653 Xavier, R.J., Wijmenga, C., Joosten, L.A.B., et al. (2018). BCG Vaccination Protects against
654 Experimental Viral Infection in Humans through the Induction of Cytokines Associated with
655 Trained Immunity. Cell Host Microbe. 23(1), 89-100 e105. Published online 2018/01/13
656 DOI: 10.1016/j.chom.2017.12.010.
657 Awuh, J.A., and Flo, T.H. (2017). Molecular basis of mycobacterial survival in macrophages.
658 Cell. Mol. Life Sci. 74(9), 1625-1648. Published online 2016/11/21 DOI: 10.1007/s00018-
659 016-2422-8.
660 Barski, A., Cuddapah, S., Kartashov, A.V., Liu, C., Imamichi, H., Yang, W., Peng, W., Lane,
661 H.C., and Zhao, K. (2017). Rapid Recall Ability of Memory T cells is Encoded in their
662 Epigenome. Sci. Rep. 7, 39785. Published online 2017/01/06 DOI: 10.1038/srep39785.
663 Benjamini, Y., and Hochberg, Y. (1995). Controlling the false discovery rate - a practical and
664 powerful approach to multiple testing. J. R. Stat. Soc. Ser. B Method. 57(1), 289-300.
665 Berry, M.P., Graham, C.M., McNab, F.W., Xu, Z., Bloch, S.A., Oni, T., Wilkinson, K.A.,
666 Banchereau, R., Skinner, J., Wilkinson, R.J., et al. (2010). An interferon-inducible
667 neutrophil-driven blood transcriptional signature in human tuberculosis. Nature. 466(7309),
668 973-977. Published online 2010/08/21 DOI: 10.1038/nature09247.
669 Bierne, H., Hamon, M., and Cossart, P. (2012). Epigenetics and bacterial infections. Cold
670 Spring Harb Perspect Med. 2(12), a010272. Published online 2012/12/05 DOI:
671 10.1101/cshperspect.a010272.
672 BoseDasgupta, S., and Pieters, J. (2018). Macrophage-microbe interaction: lessons learned
673 from the pathogen *Mycobacterium tuberculosis*. Semin. Immunopathol. 40(6), 577-591.
674 Published online 2018/10/12 DOI: 10.1007/s00281-018-0710-0.
675 Bouttier, M., Laperriere, D., Memari, B., Mangiapane, J., Fiore, A., Mitchell, E., Verway, M.,
676 Behr, M.A., Sladek, R., Barreiro, L.B., et al. (2016). Alu repeats as transcriptional regulatory

677 platforms in macrophage responses to *M. tuberculosis* infection. Nucleic Acids Res. 44(22),
678 10571-10587. Published online 2016/09/09 DOI: 10.1093/nar/gkw782.
679 Boxx, G.M., and Cheng, G. (2016). The Roles of Type I Interferon in Bacterial Infection.
680 Cell Host Microbe. 19(6), 760-769. Published online 2016/06/10 DOI:
681 10.1016/j.chom.2016.05.016.
682 Buddle, B.M., Vordermeier, H.M., and Hewinson, R.G. (2016). Experimental infection
683 models of tuberculosis in domestic livestock. Microbiol. Spectr. 4(4). Published online
684 2016/10/12 DOI: 10.1128/microbiolspec.TBTB2-0017-2016.
685 Cambier, C.J., Falkow, S., and Ramakrishnan, L. (2014). Host evasion and exploitation
686 schemes of *Mycobacterium tuberculosis*. Cell. 159(7), 1497-1509. Published online
687 2014/12/20 DOI: 10.1016/j.cell.2014.11.024.
688 Charrel-Dennis, M., Latz, E., Halmen, K.A., Trieu-Cuot, P., Fitzgerald, K.A., Kasper, D.L.,
689 and Golenbock, D.T. (2008). TLR-independent type I interferon induction in response to an
690 extracellular bacterial pathogen via intracellular recognition of its DNA. Cell Host Microbe.
691 4(6), 543-554. Published online 2008/12/10 DOI: 10.1016/j.chom.2008.11.002.
692 Chaurasiya, S.K. (2018). Tuberculosis: Smart manipulation of a lethal host. Microbiol.
693 Immunol. 62(6), 361-379. Published online 2018/04/25 DOI: 10.1111/1348-0421.12593.
694 Cheng, J., Blum, R., Bowman, C., Hu, D., Shilatifard, A., Shen, S., and Dynlacht, B.D.
695 (2014). A role for H3K4 monomethylation in gene repression and partitioning of chromatin
696 readers. Mol. Cell. 53(6), 979-992. Published online 2014/03/25 DOI:
697 10.1016/j.molcel.2014.02.032.
698 Cliff, J.M., Kaufmann, S.H., McShane, H., van Helden, P., and O'Garra, A. (2015). The
699 human immune response to tuberculosis and its treatment: a view from the blood. Immunol.
700 Rev. 264(1), 88-102. Published online 2015/02/24 DOI: 10.1111/imr.12269.
701 Clouaire, T., Webb, S., Skene, P., Illingworth, R., Kerr, A., Andrews, R., Lee, J.H., Skalnik,
702 D., and Bird, A. (2012). Cfp1 integrates both CpG content and gene activity for accurate
703 H3K4me3 deposition in embryonic stem cells. Genes Dev. 26(15), 1714-1728. Published
704 online 2012/08/03 DOI: 10.1101/gad.194209.112.
705 de Chastellier, C. (2009). The many niches and strategies used by pathogenic mycobacteria
706 for survival within host macrophages. Immunobiology. 214(7), 526-542. Published online
707 2009/03/06 DOI: 10.1016/j.imbio.2008.12.005.
708 Dixit, E., and Kagan, J.C. (2013). Intracellular pathogen detection by RIG-I-like receptors.
709 Adv. Immunol. 117, 99-125. Published online 2013/04/25 DOI: 10.1016/B978-0-12-410524-
710 9.00004-9.

711 Ehrt, S., and Schnappinger, D. (2009). Mycobacterial survival strategies in the phagosome:
712 defence against host stresses. Cell. Microbiol. 11(8), 1170-1178. Published online 2009/05/15
713 DOI: CMI1335 [pii]
714 10.1111/j.1462-5822.2009.01335.x.
715 Feng, J., Liu, T., and Zhang, Y. (2011). Using MACS to identify peaks from ChIP-Seq data.
716 Current protocols in bioinformatics. Chapter 2, Unit 2 14. Published online 2011/06/03 DOI:
717 10.1002/0471250953.bi0214s34.
718 Fitzgerald, S.D., and Kaneene, J.B. (2013). Wildlife reservoirs of bovine tuberculosis
719 worldwide: hosts, pathology, surveillance, and control. Vet. Pathol. 50(3), 488-499.
720 Published online 2012/11/22 DOI: 10.1177/0300985812467472.
721 Garnier, T., Eiglmeier, K., Camus, J.C., Medina, N., Mansoor, H., Pryor, M., Duthoy, S.,
722 Grondin, S., Lacroix, C., Monsempe, C., et al. (2003). The complete genome sequence of
723 *Mycobacterium bovis*. Proc. Natl. Acad. Sci. U. S. A. 100(13), 7877-7882. Published online
724 2003/06/06 DOI: 10.1073/pnas.1130426100.
725 Gormley, E., and Corner, L.A.L. (2017). Pathogenesis of *Mycobacterium bovis* infection: the
726 badger model as a paradigm for understanding tuberculosis in animals. Front. Vet. Sci. 4,
727 247. Published online 2018/01/31 DOI: 10.3389/fvets.2017.00247.
728 Hamon, M.A., and Cossart, P. (2008). Histone modifications and chromatin remodeling
729 during bacterial infections. Cell Host Microbe. 4(2), 100-109. Published online 2008/08/12
730 DOI: 10.1016/j.chom.2008.07.009.
731 Hardbower, D.M., Asim, M., Murray-Stewart, T., Casero, R.A., Jr., Verriere, T., Lewis,
732 N.D., Chaturvedi, R., Piazuelo, M.B., and Wilson, K.T. (2016). Arginase 2 deletion leads to
733 enhanced M1 macrophage activation and upregulated polyamine metabolism in response to
734 Helicobacter pylori infection. Amino Acids. 48(10), 2375-2388. Published online 2016/04/15
735 DOI: 10.1007/s00726-016-2231-2.
736 Huang da, W., Sherman, B.T., and Lempicki, R.A. (2009). Systematic and integrative
737 analysis of large gene lists using DAVID bioinformatics resources. Nat. Protoc. 4(1), 44-57.
738 Published online 2009/01/10 DOI: 10.1038/nprot.2008.211.
739 Huang, Z., Luo, Q., Guo, Y., Chen, J., Xiong, G., Peng, Y., Ye, J., and Li, J. (2015).
740 Mycobacterium tuberculosis-Induced Polarization of Human Macrophage Orchestrates the
741 Formation and Development of Tuberculous Granulomas In Vitro. PLoS ONE. 10(6),
742 e0129744. Published online 2015/06/20 DOI: 10.1371/journal.pone.0129744.

743 Hussain Bhat, K., and Mukhopadhyay, S. (2015). Macrophage takeover and the host-bacilli
744 interplay during tuberculosis. Future Microbiol. 10(5), 853-872. Published online 2015/05/23
745 DOI: 10.2217/fmb.15.11.
746 Jensen, K., Gallagher, I.J., Johnston, N., Welsh, M., Skuce, R., Williams, J.L., and Glass, E.J.
747 (2018). Variation in the early host-pathogen interaction of bovine macrophages with
748 divergent *Mycobacterium bovis* strains in the United Kingdom. Infect. Immun. 86(3).
749 Published online 2017/12/22 DOI: 10.1128/iai.00385-17.
750 Kaufmann, S.H.E., and Dorhoi, A. (2016). Molecular determinants in phagocyte-bacteria
751 interactions. Immunity. 44(3), 476-491. Published online 2016/03/18 DOI:
752 10.1016/j.immuni.2016.02.014.
753 Kramer, A., Green, J., Pollard, J., Jr., and Tugendreich, S. (2014). Causal analysis approaches
754 in Ingenuity Pathway Analysis. Bioinformatics. 30(4), 523-530. Published online 2013/12/18
755 DOI: 10.1093/bioinformatics/btt703.
756 LaMere, S.A., Thompson, R.C., Komori, H.K., Mark, A., and Salomon, D.R. (2016).
757 Promoter H3K4 methylation dynamically reinforces activation-induced pathways in human
758 CD4 T cells. Genes Immun. 17(5), 283-297. Published online 2016/05/14 DOI:
759 10.1038/gene.2016.19.
760 Landt, S.G., Marinov, G.K., Kundaje, A., Kheradpour, P., Pauli, F., Batzoglou, S., Bernstein,
761 B.E., Bickel, P., Brown, J.B., Cayting, P., et al. (2012). ChIP-seq guidelines and practices of
762 the ENCODE and modENCODE consortia. Genome Res. 22(9), 1813-1831. Published online
763 2012/09/08 DOI: 10.1101/gr.136184.111.
764 Langmead, B., and Salzberg, S.L. (2012). Fast gapped-read alignment with Bowtie 2. Nat.
765 Methods. 9(4), 357-359. Published online 2012/03/06 DOI: 10.1038/nmeth.1923.
766 Lavalett, L., Rodriguez, H., Ortega, H., Sadee, W., Schlesinger, L.S., and Barrera, L.F.
767 (2017). Alveolar macrophages from tuberculosis patients display an altered inflammatory
768 gene expression profile. Tuberculosis. 107(Supplement C), 156-167. DOI:
769 https://doi.org/10.1016/j.tube.2017.08.012.
770 Lerdrup, M., Johansen, J.V., Agrawal-Singh, S., and Hansen, K. (2016). An interactive
771 environment for agile analysis and visualization of ChIP-sequencing data. Nat. Struct. Mol.
772 Biol. 23(4), 349-357. Published online 2016/03/02 DOI: 10.1038/nsmb.3180.
773 Lewis, N.D., Asim, M., Barry, D.P., de Sablet, T., Singh, K., Piazuelo, M.B., Gobert, A.P.,
774 Chaturvedi, R., and Wilson, K.T. (2011). Immune evasion by Helicobacter pylori is mediated
775 by induction of macrophage arginase II. J. Immunol. 186(6), 3632-3641. Published online
776 2011/02/08 DOI: 10.4049/jimmunol.1003431.

Li, H., Handsaker, B., Wysoker, A., Fennell, T., Ruan, J., Homer, N., Marth, G., Abecasis, G., Durbin, R., and Genome Project Data Processing, S. (2009). The Sequence Alignment/Map format and SAMtools. Bioinformatics. 25(16), 2078-2079. Published online 2009/06/10 DOI: 10.1093/bioinformatics/btp352.

Loo, Y.M., and Gale, M., Jr. (2011). Immune signaling by RIG-I-like receptors. Immunity. 34(5), 680-692. Published online 2011/05/28 DOI: 10.1016/j.immuni.2011.05.003.

Love, M.I., Huber, W., and Anders, S. (2014). Moderated estimation of fold change and dispersion for RNA-seq data with DESeq2. Genome Biol. 15(12), 550. Published online 2014/12/18 DOI: 10.1186/s13059-014-0550-8.

Magee, D.A., Conlon, K.M., Nalpas, N.C., Browne, J.A., Pirson, C., Healy, C., McLoughlin, K.E., Chen, J., Vordermeier, H.M., Gormley, E., et al. (2014). Innate cytokine profiling of bovine alveolar macrophages reveals commonalities and divergence in the response to Mycobacterium bovis and Mycobacterium tuberculosis infection. Tuberculosis (Edinb). 94(4), 441-450. Published online 2014/06/03 DOI: 10.1016/j.tube.2014.04.004.

Malone, K.M., and Gordon, S.V. (2017). *Mycobacterium tuberculosis* complex members adapted to wild and domestic animals. Adv. Exp. Med. Biol. 1019, 135-154. Published online 2017/11/09 DOI: 10.1007/978-3-319-64371-7_7.

Malone, K.M., Rue-Albrecht, K., Magee, D.A., Conlon, K., Schubert, O.T., Nalpas, N.C., Browne, J.A., Smyth, A., Gormley, E., Aebersold, R., et al. (2018). Comparative 'omics analyses differentiate *Mycobacterium tuberculosis* and *Mycobacterium bovis* and reveal distinct macrophage responses to infection with the human and bovine tubercle bacilli. Microb. Genom., [Epub ahead of print]. Published online 2018/03/21 DOI: 10.1099/mgen.0.000163.

Manca, C., Tsenova, L., Bergtold, A., Freeman, S., Tovey, M., Musser, J.M., Barry, C.E., 3rd, Freedman, V.H., and Kaplan, G. (2001). Virulence of a Mycobacterium tuberculosis clinical isolate in mice is determined by failure to induce Th1 type immunity and is associated with induction of IFN-alpha /beta. Proc. Natl. Acad. Sci. U. S. A. 98(10), 5752-5757. Published online 2001/04/26 DOI: 10.1073/pnas.091096998.

Manca, C., Tsenova, L., Freeman, S., Barczak, A.K., Tovey, M., Murray, P.J., Barry, C., and Kaplan, G. (2005). Hypervirulent M. tuberculosis W/Beijing strains upregulate type I IFNs and increase expression of negative regulators of the Jak-Stat pathway. J. Interferon Cytokine Res. 25(11), 694-701. Published online 2005/12/02 DOI: 10.1089/jir.2005.25.694.

Mancuso, G., Midiri, A., Biondo, C., Beninati, C., Zummo, S., Galbo, R., Tomasello, F., Gambuzza, M., Macri, G., Ruggeri, A., et al. (2007). Type I IFN signaling is crucial for host

resistance against different species of pathogenic bacteria. J. Immunol. 178(5), 3126-3133. Published online 2007/02/22.

Manzanillo, P.S., Shiloh, M.U., Portnoy, D.A., and Cox, J.S. (2012). Mycobacterium tuberculosis activates the DNA-dependent cytosolic surveillance pathway within macrophages. Cell Host Microbe. 11(5), 469-480. Published online 2012/05/23 DOI: 10.1016/j.chom.2012.03.007.

Marino, V.J., and Roguin, L.P. (2008). The granulocyte colony stimulating factor (G-CSF) activates Jak/STAT and MAPK pathways in a trophoblastic cell line. J. Cell. Biochem. 103(5), 1512-1523. Published online 2007/09/21 DOI: 10.1002/jcb.21542.

Marr, A.K., MacIsaac, J.L., Jiang, R., Airo, A.M., Kobor, M.S., and McMaster, W.R. (2014). *Leishmania donovani* infection causes distinct epigenetic DNA methylation changes in host macrophages. PLoS Pathog. 10(10), e1004419. Published online 2014/10/10 DOI: 10.1371/journal.ppat.1004419.

Martin, M. (2011). Cutadapt removes adapter sequences from high-throughput sequencing reads. 2011. 17(1), 3. Published online 2011-08-02 DOI: 10.14806/ej.17.1.200.

Martins, A., Han, J., and Kim, S.O. (2010). The multifaceted effects of granulocyte colony-stimulating factor in immunomodulation and potential roles in intestinal immune homeostasis. IUBMB Life. 62(8), 611-617. Published online 2010/08/04 DOI: 10.1002/iub.361.

Mayer-Barber, K.D., Andrade, B.B., Oland, S.D., Amaral, E.P., Barber, D.L., Gonzales, J., Derrick, S.C., Shi, R., Kumar, N.P., Wei, W., et al. (2014). Host-directed therapy of tuberculosis based on interleukin-1 and type I interferon crosstalk. Nature. 511(7507), 99-103. Published online 2014/07/06 DOI: 10.1038/nature13489.

McNab, F., Mayer-Barber, K., Sher, A., Wack, A., and O'Garra, A. (2015). Type I interferons in infectious disease. Nat. Rev. Immunol. 15(2), 87-103. Published online 2015/01/24 DOI: 10.1038/nri3787.

Meenu, S., Thiagarajan, S., Ramalingam, S., Michael, A., and Ramalingam, S. (2016). Modulation of host ubiquitin system genes in human endometrial cell line infected with Mycobacterium tuberculosis. Med Microbiol Immunol. 205(2), 163-171. Published online 2015/09/26 DOI: 10.1007/s00430-015-0432-z.

Mi, H., Huang, X., Muruganujan, A., Tang, H., Mills, C., Kang, D., and Thomas, P.D. (2017). PANTHER version 11: expanded annotation data from Gene Ontology and Reactome pathways, and data analysis tool enhancements. Nucleic Acids Res. 45(D1), D183-D189. Published online 2016/12/03 DOI: 10.1093/nar/gkw1138.

Nalpas, N.C., Magee, D.A., Conlon, K.M., Browne, J.A., Healy, C., McLoughlin, K.E., Rue-Albrecht, K., McGettigan, P.A., Killick, K.E., Gormley, E., et al. (2015). RNA sequencing provides exquisite insight into the manipulation of the alveolar macrophage by tubercle bacilli. Sci. Rep. 5, 13629. Published online 2015/09/09 DOI: 10.1038/srep13629.

Nepal, R.M., Mampe, S., Shaffer, B., Erickson, A.H., and Bryant, P. (2006). Cathepsin L maturation and activity is impaired in macrophages harboring M. avium and M. tuberculosis. Int. Immunol. 18(6), 931-939. Published online 2006/04/26 DOI: 10.1093/intimm/dxl029.

Niller, H.H., and Minarovits, J. (2016). Patho-epigenetics of infectious diseases caused by intracellular bacteria. Adv. Exp. Med. Biol. 879, 107-130. Published online 2015/12/15 DOI: 10.1007/978-3-319-24738-0_6.

O'Connell, R.M., Saha, S.K., Vaidya, S.A., Bruhn, K.W., Miranda, G.A., Zarnegar, B., Perry, A.K., Nguyen, B.O., Lane, T.F., Taniguchi, T., et al. (2004). Type I interferon production enhances susceptibility to Listeria monocytogenes infection. J. Exp. Med. 200(4), 437-445. Published online 2004/08/11 DOI: 10.1084/jem.20040712.

O'Doherty, A.M., O'Shea, L.C., and Fair, T. (2012). Bovine DNA methylation imprints are established in an oocyte size-specific manner, which are coordinated with the expression of the DNMT3 family proteins. Biol. Reprod. 86(3), 67. Published online 2011/11/18 DOI: 10.1095/biolreprod.111.094946.

O'Kane, C.M., Elkington, P.T., and Friedland, J.S. (2008). Monocyte-dependent oncostatin M and TNF-alpha synergize to stimulate unopposed matrix metalloproteinase-1/3 secretion from human lung fibroblasts in tuberculosis. Eur. J. Immunol. 38(5), 1321-1330. Published online 2008/04/10 DOI: 10.1002/eji.200737855.

Olea-Popelka, F., Muwonge, A., Perera, A., Dean, A.S., Mumford, E., Erlacher-Vindel, E., Forcella, S., Silk, B.J., Ditiu, L., El Idrissi, A., et al. (2017). Zoonotic tuberculosis in human beings caused by *Mycobacterium bovis* – a call for action. Lancet Infect. Dis. 17(1), e21-e25. Published online 2016/10/05 DOI: 10.1016/S1473-3099(16)30139-6.

Palmer, M.V. (2013). *Mycobacterium bovis*: characteristics of wildlife reservoir hosts. Transbound. Emerg. Dis. 60 Suppl 1, 1-13. Published online 2013/11/06 DOI: 10.1111/tbed.12115.

Papp, A.C., Azad, A.K., Pietrzak, M., Williams, A., Handelman, S.K., Igo, R.P., Jr., Stein, C.M., Hartmann, K., Schlesinger, L.S., and Sadee, W. (2018). AmpliSeq transcriptome analysis of human alveolar and monocyte-derived macrophages over time in response to *Mycobacterium tuberculosis* infection. PLoS ONE. 13(5), e0198221. Published online 2018/05/31 DOI: 10.1371/journal.pone.0198221.

879 Pastuschek, J., Poetzsch, J., Morales-Prieto, D.M., Schleussner, E., Markert, U.R., and
880 Georgiev, G. (2015). Stimulation of the JAK/STAT pathway by LIF and OSM in the human
881 granulosa cell line COV434. J. Reprod. Immunol. 108, 48-55. Published online 2015/03/31
882 DOI: 10.1016/j.jri.2015.03.002.
883 Patro, R., Duggal, G., Love, M.I., Irizarry, R.A., and Kingsford, C. (2017). Salmon provides
884 fast and bias-aware quantification of transcript expression. Nat. Methods. 14(4), 417-419.
885 Published online 2017/03/07 DOI: 10.1038/nmeth.4197.
886 Pennini, M.E., Perrinet, S., Dautry-Varsat, A., and Subtil, A. (2010). Histone methylation by
887 NUE, a novel nuclear effector of the intracellular pathogen *Chlamydia trachomatis*. PLoS
888 Pathog. 6(7), e1000995. Published online 2010/07/27 DOI: 10.1371/journal.ppat.1000995.
889 Polena, H., Boudou, F., Tilleul, S., Dubois-Colas, N., Lecointe, C., Rakotosamimanana, N.,
890 Pelizzola, M., Andriamandimby, S.F., Raharimanga, V., Charles, P., et al. (2016).
891 Mycobacterium tuberculosis exploits the formation of new blood vessels for its
892 dissemination. Sci. Rep. 6, 33162. Published online 2016/09/13 DOI: 10.1038/srep33162.
893 Queval, C.J., Brosch, R., and Simeone, R. (2017). The macrophage: A disputed fortress in the
894 battle against *Mycobacterium tuberculosis*. Front. Microbiol. 8, 2284. Published online
895 2017/12/09 DOI: 10.3389/fmicb.2017.02284.
896 Rawlings, J.S., Rosler, K.M., and Harrison, D.A. (2004). The JAK/STAT signaling pathway.
897 J. Cell Sci. 117(Pt 8), 1281-1283. Published online 2004/03/17 DOI: 10.1242/jcs.00963.
898 Richardson, I.W., Berry, D.P., Wiencko, H.L., Higgins, I.M., More, S.J., McClure, J., Lynn,
899 D.J., and Bradley, D.G. (2016). A genome-wide association study for genetic susceptibility to
900 Mycobacterium bovis infection in dairy cattle identifies a susceptibility QTL on chromosome
901 23. Genet Sel Evol. 48, 19. Published online 2016/03/11 DOI: 10.1186/s12711-016-0197-x.
902 Rolando, M., Gomez-Valero, L., and Buchrieser, C. (2015). Bacterial remodelling of the host
903 epigenome: functional role and evolution of effectors methylating host histones. Cell.
904 Microbiol. 17(8), 1098-1107. Published online 2015/06/03 DOI: 10.1111/cmi.12463.
905 Rolando, M., Sanulli, S., Rusniok, C., Gomez-Valero, L., Bertholet, C., Sahr, T., Margueron,
906 R., and Buchrieser, C. (2013). Legionella pneumophila effector RomA uniquely modifies
907 host chromatin to repress gene expression and promote intracellular bacterial replication. Cell
908 Host Microbe. 13(4), 395-405. Published online 2013/04/23 DOI:
909 10.1016/j.chom.2013.03.004.
910 Schorey, J.S., and Schlesinger, L.S. (2016). Innate immune responses to tuberculosis.
911 Microbiol. Spectr. 4(6). Published online 2017/01/15 DOI: 10.1128/microbiolspec.TBTB2-
912 0010-2016.

913 Sharma, G., Sowpati, D.T., Singh, P., Khan, M.Z., Ganji, R., Upadhyay, S., Banerjee, S.,
914 Nandicoori, V.K., and Khosla, S. (2016). Genome-wide non-CpG methylation of the host
915 genome during M. tuberculosis infection. Sci. Rep. 6, 25006. Published online 2016/04/27
916 DOI: 10.1038/srep25006.
917 Sharma, G., Upadhyay, S., Srilalitha, M., Nandicoori, V.K., and Khosla, S. (2015). The
918 interaction of mycobacterial protein Rv2966c with host chromatin is mediated through non-
919 CpG methylation and histone H3/H4 binding. Nucleic Acids Res. 43(8), 3922-3937.
920 Published online 2015/04/01 DOI: 10.1093/nar/gkv261.
921 Silmon de Monerri, N.C., and Kim, K. (2014). Pathogens hijack the epigenome: a new twist
922 on host-pathogen interactions. Am. J. Pathol. 184(4), 897-911. Published online 2014/02/15
923 DOI: 10.1016/j.ajpath.2013.12.022.
924 Silver, R.F., Walrath, J., Lee, H., Jacobson, B.A., Horton, H., Bowman, M.R., Nocka, K., and
925 Sypek, J.P. (2009). Human alveolar macrophage gene responses to Mycobacterium
926 tuberculosis strains H37Ra and H37Rv. Am. J. Respir. Cell Mol. Biol. 40(4), 491-504.
927 Published online 2008/09/13 DOI: 10.1165/rcmb.2008-0219OC.
928 Sims, R.J., 3rd, Nishioka, K., and Reinberg, D. (2003). Histone lysine methylation: a
929 signature for chromatin function. Trends Genet. 19(11), 629-639. Published online
930 2003/10/31 DOI: 10.1016/j.tig.2003.09.007.
931 Soneson, C., Love, M.I., and Robinson, M.D. (2015). Differential analyses for RNA-seq:
932 transcript-level estimates improve gene-level inferences. F1000Research. 4, 1521. Published
933 online 2016/03/01 DOI: 10.12688/f1000research.7563.2.
934 Stark, R., and Brown, G., 2011. DiffBind: differential binding analysis of ChIP-Seq peak
935 data. http://bioconductor.org/packages/release/bioc/vignettes/DiffBind/inst/doc/DiffBind.pdf.
936 Steele, J.H. (1995). Introduction (Part 2 Regional and Country Status Reports). In:
937 *Mycobacterium bovis* infection in animals and humans, C.O. Thoen, and J.H. Steele eds.
938 (Iowa State University Press, Ames, IA, USA), pp. 169-172.
939 Stutz, M.D., Clark, M.P., Doerflinger, M., and Pellegrini, M. (2018). *Mycobacterium*
940 *tuberculosis*: Rewiring host cell signaling to promote infection. J. Leukoc. Biol. 103(2), 259-
941 268. Published online 2018/01/19 DOI: 10.1002/JLB.4MR0717-277R.
942 Thoen, C.O., Kaplan, B., Thoen, T.C., Gilsdorf, M.J., and Shere, J.A. (2016). Zoonotic
943 tuberculosis. A comprehensive ONE HEALTH approach. Medicina (B Aires). 76(3), 159-
944 165. Published online 2016/06/14.
945 Thomas, P.D., Campbell, M.J., Kejariwal, A., Mi, H., Karlak, B., Daverman, R., Diemer, K.,
946 Muruganujan, A., and Narechania, A. (2003). PANTHER: a library of protein families and

947 subfamilies indexed by function. Genome Res. 13(9), 2129-2141. Published online
948 2003/09/04 DOI: 10.1101/gr.772403.
949 Thorvaldsdottir, H., Robinson, J.T., and Mesirov, J.P. (2013). Integrative Genomics Viewer
950 (IGV): high-performance genomics data visualization and exploration. Brief. Bioinform.
951 14(2), 178-192. Published online 2012/04/21 DOI: 10.1093/bib/bbs017.
952 Tsumura, M., Okada, S., Sakai, H., Yasunaga, S., Ohtsubo, M., Murata, T., Obata, H.,
953 Yasumi, T., Kong, X.F., Abhyankar, A., et al. (2012). Dominant-negative STAT1 SH2
954 domain mutations in unrelated patients with Mendelian susceptibility to mycobacterial
955 disease. Hum. Mutat. 33(9), 1377-1387. Published online 2012/05/11 DOI:
956 10.1002/humu.22113.
957 Vayr, F., Martin-Blondel, G., Savall, F., Soulat, J.M., Deffontaines, G., and Herin, F. (2018).
958 Occupational exposure to human *Mycobacterium bovis* infection: A systematic review. PLoS
959 Negl. Trop. Dis. 12(1), e0006208. Published online 2018/01/18 DOI:
960 10.1371/journal.pntd.0006208.
961 Vegh, P., Foroushani, A.B., Magee, D.A., McCabe, M.S., Browne, J.A., Nalpas, N.C.,
962 Conlon, K.M., Gordon, S.V., Bradley, D.G., MacHugh, D.E., et al. (2013). Profiling
963 microRNA expression in bovine alveolar macrophages using RNA-seq. Vet. Immunol.
964 Immunopathol. 155(4), 238-244. Published online 2013/09/12 DOI:
965 10.1016/j.vetimm.2013.08.004.
966 Vegh, P., Magee, D.A., Nalpas, N.C., Bryan, K., McCabe, M.S., Browne, J.A., Conlon,
967 K.M., Gordon, S.V., Bradley, D.G., MacHugh, D.E., et al. (2015). MicroRNA profiling of the
968 bovine alveolar macrophage response to *Mycobacterium bovis* infection suggests pathogen
969 survival is enhanced by microRNA regulation of endocytosis and lysosome trafficking.
970 Tuberculosis. 95(1), 60-67. DOI: 10.1016/j.tube.2014.10.011.
971 Vejnar, C.E., and Zdobnov, E.M. (2012). MiRmap: comprehensive prediction of microRNA
972 target repression strength. Nucleic Acids Res. 40(22), 11673-11683. Published online
973 2012/10/05 DOI: 10.1093/nar/gks901.
974 Vernimmen, D., Lynch, M.D., De Gobbi, M., Garrick, D., Sharpe, J.A., Sloane-Stanley, J.A.,
975 Smith, A.J., and Higgs, D.R. (2011). Polycomb eviction as a new distant enhancer function.
976 Genes Dev. 25(15), 1583-1588. Published online 2011/08/11 DOI: 10.1101/gad.16985411.
977 Vogler, M. (2012). BCL2A1: the underdog in the BCL2 family. Cell Death Differ. 19(1), 67-
978 74. Published online 2011/11/15 DOI: 10.1038/cdd.2011.158.
979 Waters, W.R., Maggioli, M.F., McGill, J.L., Lyashchenko, K.P., and Palmer, M.V. (2014).
980 Relevance of bovine tuberculosis research to the understanding of human disease: historical

perspectives, approaches, and immunologic mechanisms. Vet. Immunol. Immunopathol. 159(3-4), 113-132. Published online 2014/03/19 DOI: 10.1016/j.vetimm.2014.02.009.

Waters, W.R., Palmer, M.V., Buddle, B.M., and Vordermeier, H.M. (2012). Bovine tuberculosis vaccine research: historical perspectives and recent advances. Vaccine. 30(16), 2611-2622. Published online 2012/02/22 DOI: 10.1016/j.vaccine.2012.02.018.

Weichhart, T., and Saemann, M.D. (2008). The PI3K/Akt/mTOR pathway in innate immune cells: emerging therapeutic applications. Ann. Rheum. Dis. 67 Suppl 3, iii70-74. Published online 2008/12/17 DOI: 10.1136/ard.2008.098459.

Weiss, G., and Schaible, U.E. (2015). Macrophage defense mechanisms against intracellular bacteria. Immunol. Rev. 264(1), 182-203. Published online 2015/02/24 DOI: 10.1111/imr.12266.

Wilbanks, E.G., and Facciotti, M.T. (2010). Evaluation of algorithm performance in ChIP-seq peak detection. PLoS ONE. 5(7), e11471. Published online 2010/07/16 DOI: 10.1371/journal.pone.0011471.

Williams, A., and Orme, I.M. (2016). Animal models of tuberculosis: an overview. Microbiol. Spectr. 4(4). Published online 2016/10/12 DOI: 10.1128/microbiolspec.TBTB2-0004-2015.

Woo, V., and Alenghat, T. (2017). Host-microbiota interactions: epigenomic regulation. Curr. Opin. Immunol. 44, 52-60. Published online 2017/01/20 DOI: 10.1016/j.coi.2016.12.001.

Yaseen, I., Kaur, P., Nandicoori, V.K., and Khosla, S. (2015). Mycobacteria modulate host epigenetic machinery by Rv1988 methylation of a non-tail arginine of histone H3. Nat. Commun. 6, 8922. Published online 2015/11/17 DOI: 10.1038/ncomms9922.

Yip, S.C., El-Sibai, M., Coniglio, S.J., Mouneimne, G., Eddy, R.J., Drees, B.E., Neilsen, P.O., Goswami, S., Symons, M., Condeelis, J.S., et al. (2007). The distinct roles of Ras and Rac in PI 3-kinase-dependent protrusion during EGF-stimulated cell migration. J. Cell Sci. 120(Pt 17), 3138-3146. Published online 2007/08/19 DOI: 10.1242/jcs.005298.

Yu, J.S., and Cui, W. (2016). Proliferation, survival and metabolism: the role of PI3K/AKT/mTOR signalling in pluripotency and cell fate determination. Development. 143(17), 3050-3060. Published online 2016/09/01 DOI: 10.1242/dev.137075.

Zheng, L., Leung, E.T.Y., Wong, H.K., Lui, G., Lee, N., To, K.-F., Choy, K.W., Chan, R.C.Y., and Ip, M. (2016). Unraveling methylation changes of host macrophages in *Mycobacterium tuberculosis* infection. Tuberculosis. 98, 139-148. DOI: http://dx.doi.org/10.1016/j.tube.2016.03.003.

1015 **Figure 1**

1016

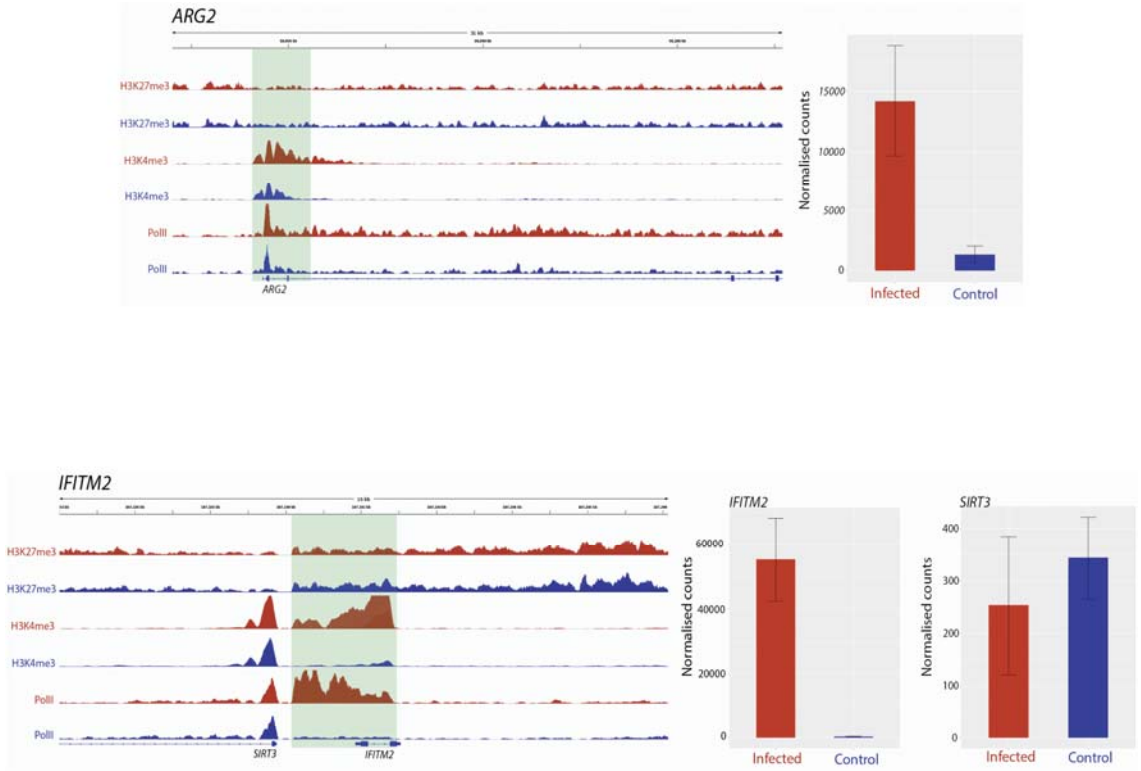

1017
1018

Figure 2

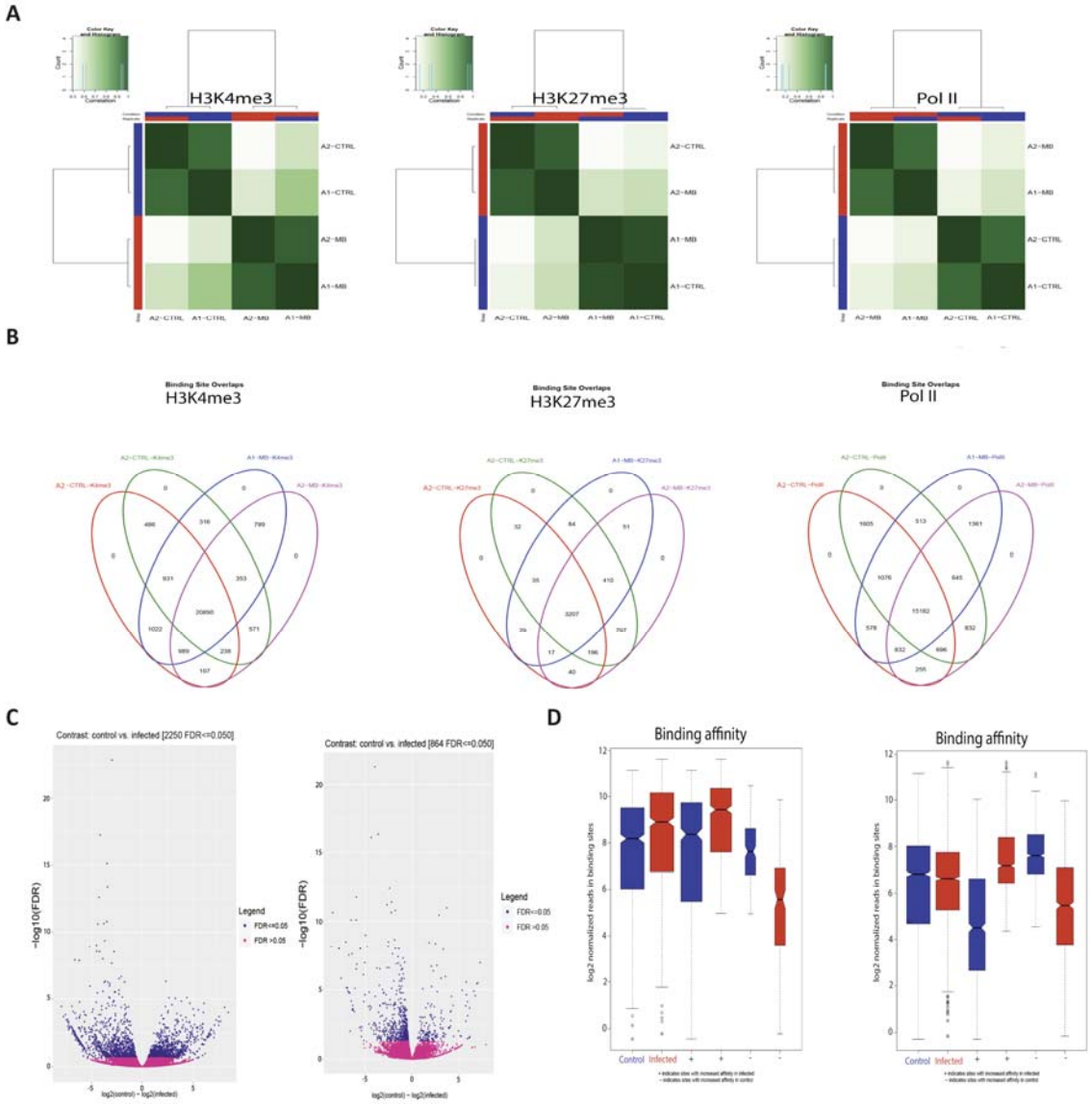

1023 **Figure 3**

1024

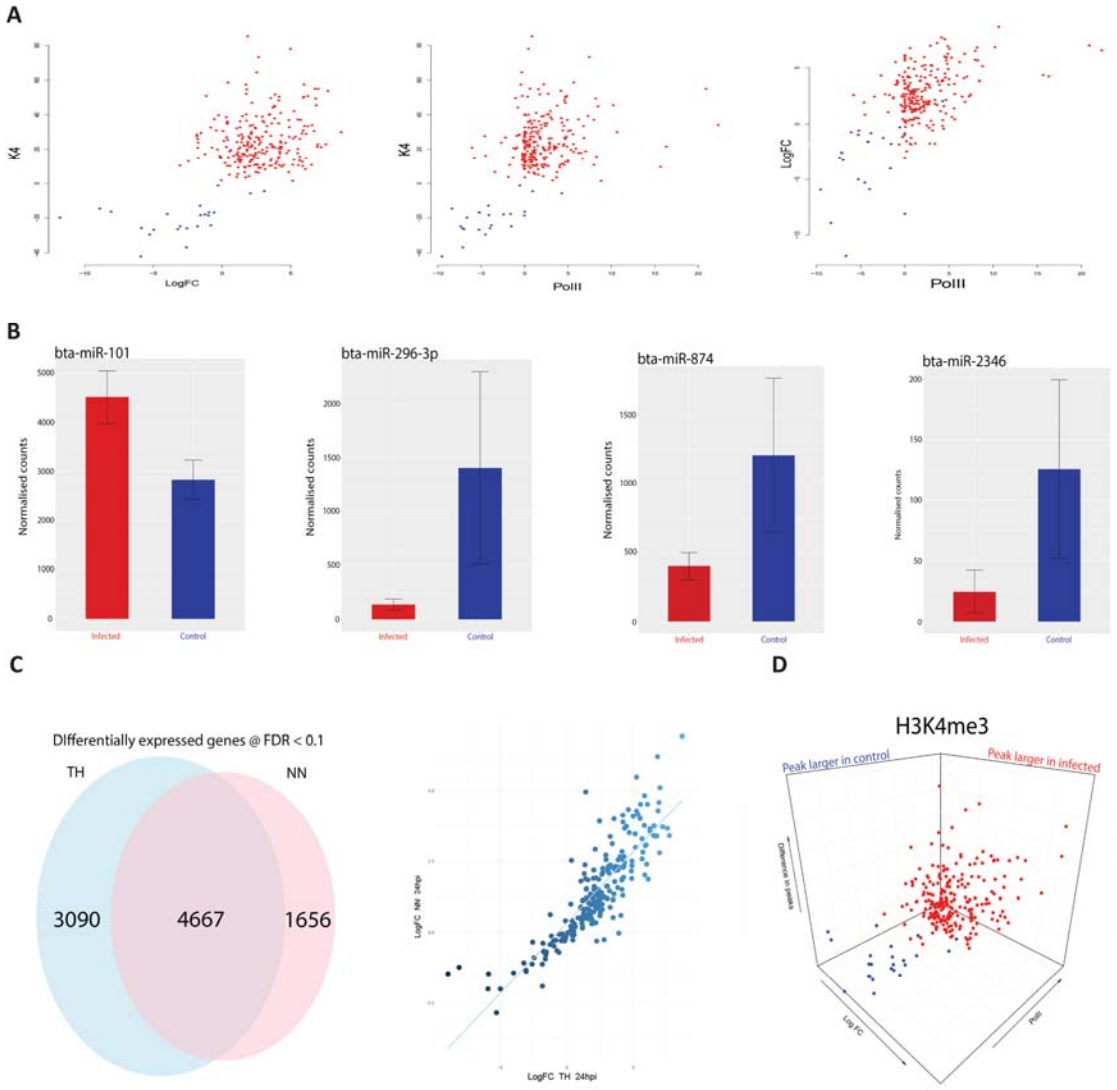

1025
1026

1027 **Figure 4**

1028

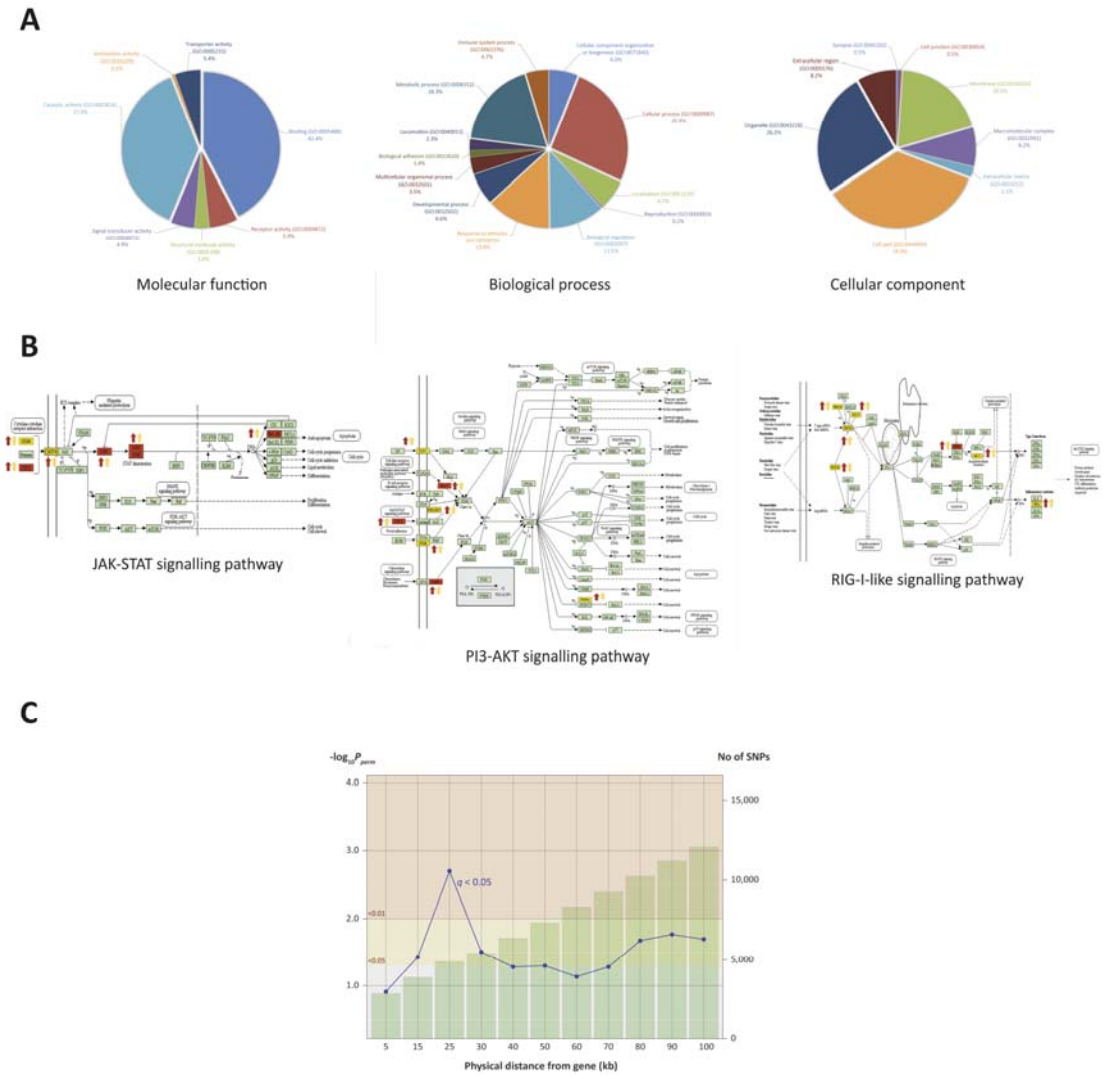

1029